2009 Third International Symposium on Intelligent Information Technology Application

An Automated Vision-Based Inspection System for Bearing Gland Covers

Jiang Guo, Duo-Yu Gu, Shu-Xiao Li, Yong-Shi Jiang and Hong-Xing Chang
Integrated Information System Research Center
Institute of Automation, Chinese Academy of Sciences
Beijing, China
{*jiang.guo, duoyu.gu, shuxiao.li, yongshi.jiang, hongxing.chang*}*@ia.ac.cn*

***Abstract*—This paper presents an automatic vision-based system for bearing gland cover quality control. The system employs the method of gradually refined scheme to locate regions of interests. Several types of defects are detected from their corresponding regions by utilizing image segmentation, curve fitting, feature validation, and other image processing methods. Although each technology is not strange to us, how to integrate them into an entire inspection system efficiently and effectively is a huge challenge. In addition, some useful visual features such as maximum of orientation difference and maximum rectangular feature are proposed to validate candidate defects. Field tests demonstrate that the proposed system gains an excellent performance.**

***Keywords*-inspection system; supervised grayscale thresholding; maximum of the orientation difference; circular analysis; maximum rectangular feature;**

I. Introduction

Industrial inspection is one of the main applications of computer vision. In the process of quality control of bearing gland covers, one important task is the detection of defects, such as burrs, gaps, color defects, rubber overflow, rust in metal, etc(see Fig.1 for example images). Up to now, the quality assessment of bearings in domestic and international enterprises is mainly based on artificial methods like random inspection, which lacks consistency and scientificity and tends to be subjected to the influence of the operator's spirits. In contrast, the vision-based method has the advantages such as high efficiency and unified criterion, which can overcome the shortages of the artificial approaches.

However, it is difficult to develop a high performance inspection system. On the one hand, an inspection system should run robust in real-time since it is usually embedded in production line. On the other hand, the users often require a very high hit rate and a low false alarm rate, which is challenging because some defects are of small size, low contrast, and less sharpness.

At present, many colleges and research institutes have devoted to the development of industrial vision-based inspection systems[1,2]. The research results are widely used in steel and coin manufacturing, which have promoted the automation level and saved lots of human resources. However, these systems are highly application related and a widely applicable system is still not available. As for the detection of gland covers, several types of defects may appear at their corresponding regions with different characteristics. Besides, the cover has two sides which needs to pay extra attention to decide the side. So, to exploit a practical system is necessary.

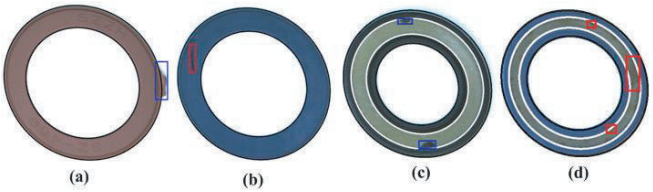

Figure 1. The main types of defects and detection resluts. (a) burr defect; (b) color defect; (c) rubber overflow defect; (d) rust defect

To address these problems, this paper presents a novel system aiming at inspecting the defects of gland covers fast and accurately. The basic approach includes two major contributions. The first one is that by integrating image segmentation, curve fitting, feature validation and other image processing technologies, an intact gland cover inspection system has been developed and put into practical use; the second one is that some useful features are proposed to complete the defect inspection task. Field test results demonstrate that the proposed system achieves a high performance and solves the online defect detection problem for gland covers.

The remainder of this paper is organized as follows. In section 2, the flowchart of the system is presented and the detection of burrs, color defects, rubber overflow defects and rust defects are described in turn. The field test results are given in section 3 prior to the conclusion in section 4.

II. Gland Cover Defect Inspection

The system includes four primary parts. The first one is gland cover image segmentation, which aim at providing the cover images for later processing. The rest is to deal with the defect inspection problems. The flowchart of the system is shown in Fig.2.

A. Gland Cover Image Segmentation

The proposed system adopts pipeline processing, that is, the conveyer belt keeps moving at a constant speed while the cameras monitor the conveyer belt in real-time and take pictures in 6 fps. The mechanical device makes sure that

978-0-7695-3859-4/09 $26.00 © 2009 IEEE
DOI 10.1109/IITA.2009.473

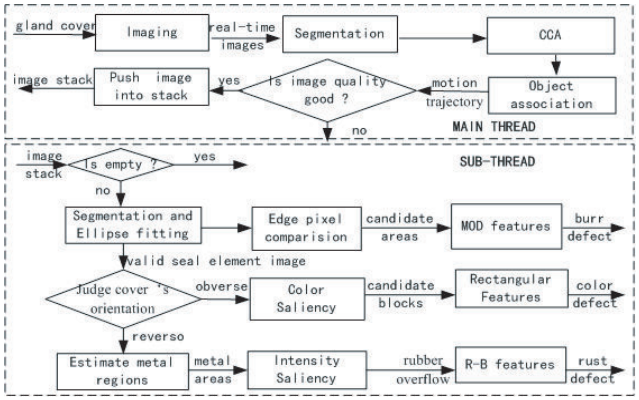

Figure 2. The flowchart of the proposed system.

the contiguous covers hold a certain distance to separate the covers from each other. The supervised grayscale thresholding [3] method is used to segment the covers.

In the obtained image sequence, the same gland cover may occur in several successive images. Thus, it is necessary to track it and select an image with better quality to be used as the input for the later stages. The data association and state estimation techniques are employed to achieve this purpose. The former aims at getting the motion trajectory based on the estimated velocity of the belt and position of the cover. The later is used to estimate the state from the trajectory to acquire the cover image whose position is in the center of the camera view. Finally, the cover image with the best quality is chosen as the output of this stage.

B. Burr Detection

A burr is the spurious boundaries which deviates from the gland cover edges. Two things make effective burr detection difficult. One is the small size, and the other is lacking of sharpness. The standard gland cover can be depicted as a circular object enclosed by two concentric circles. From that, a direct method to judge burr defect is to check whether a point fitting well to the model. However, the assumption is not always true for two cases. Firstly, the motion blur can't be neglected as the images are acquired from the moving belt. Secondly, the camera's optical axis doesn't perpendicular to the conveyer belt exactly. In order to overcome that deficiency, the ellipse model is introduced instead and the centers of the two ellipses are not coincident any more.

As the system utilizes a simple background, it's favorable for threshold based segmentation methods. Here, the supervised grayscale thresholding [3] method is adopted. After binary segmentation, the morphological filters are used for noise removal and edge extraction. The edges are refined to sub-pixel localization using moment based approach [8]. The ellipse models are acquired by fitting these points sampled from the extracted edges. Subsequently, the foreground areas

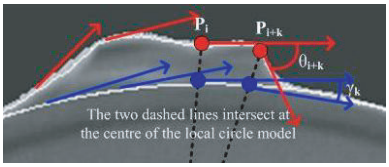

Figure 3. The explanation of orientation difference. P_i and P_{i+k} are two points at the burr contour. $\theta_{i,k}$ and γ_k are two cross angles.

which are out of the regions enclosed by the two ellipses are considered as burr candidates.

Although the means above can detect the burrs, the performance is not satisfactory since some non-burr areas may be also extracted. A further refined scheme should be incorporated. The Poincaré Index feature is defined as the sum of the orientation differences (OD) along a closed circle and it's useful for the singular points detection. Zhou.J et al.[4] indicate that when the fingerprint images contain creases, scars, smudges, the Poincaré Index based method will result in many spurious singular points. There, the authors extended the orientation differences to a vector and proposed the so called DORIC feature. Inspired by it, we use OD flexibly in burrs detection. The proposed feature is named maximum orientation differences and MOD is used for short. As shown in Fig.3, the tangential directions of the contour points change smoothly when the gland cover doesn't have burrs, but they vary drastically when the edge points are in burr regions. The sharper the burrs, the more obvious the changes.

Assume the sequential point set of the burr contour $\overline{C}$ is represented as $E_{burr} = \{p_i \in \overline{C}, i = 1, 2, ...n\}$, the OD of the two tangential directions of p_i and p_{i+k} is,

$$\theta_{i,k} = \arccos(\frac{< \vec{v}_i \cdot \vec{v}_{i+k} >}{|\vec{v}_i||\vec{v}_{i+k}|}) \tag{1}$$

where k is the index difference value between the two points, while $\vec{v}_i$ and $\vec{v}_{i+k}$ are two 2-D vectors to represent tangential directions at the two points respectively. The local contour of the cover can be viewed as a part of a circle. So, if that local contour doesn't have burr, the OD between the two points is,

$$\gamma_k = \frac{k}{r_{p_i}} \tag{2}$$

where r_{p_i} is the radius of the local circle model. From the analysis above, if p_i and p_{i+k} are not in burr regions, there is a relation $\delta\theta = |\theta_{i,k} - \gamma_k| \approx 0$. The MOD is,

$$\max_{\substack{0 \le i \le n, \\ 2 \le k \le 10}} |\theta_{i,k} - \gamma_k| \tag{3}$$

If the MOD feature of some area excesses a given threshold, it has burr defect. The burr inspection algorithm is summarized as follows:

1. Apply the thresholding method [3] and morphological filters to get the binary image and edges of gland cover.

2. Fit the sampled edge points to get the ellipse models E_{out} and E_{in} using robust fitting techniques; denote the region enclosed by these two ellipses as R_{cover}.

3. Use point by point comparison and CCA techniques to get the burr candidate areas based on the binary image and R_{cover}.

4. Compute MOD feature for each area and validate it.

Through those 4 steps, the burr detection is efficiently completed. The MOD feature is useful because it response sensitively to the changing trend of the burr contour.

C. Color Defect Detection

Color defect (CD) means the color of some area is not consistent with the standard. The difficulty to detect it lies in the non-uniform lighting and low color contrast. In order to accomplish this assignment, three cascade steps are introduced to gradually refine the results. The former two are color saliency based multi-threshold segmentation and circular analysis, which are combined to generate regions of interest. The last one is a maximum rectangular feature based validation process.

1. *Color Saliency Based Multi-threshold Segmentation.* By observing the images, a simple fact is that the areas which notably different with the standard are surely of CDs, and the areas which are quite similar with the standard are certainly not of CDs. Here, The processing regions is R_{cover} derived from section B. Transform those pixels from RGB to YIQ color space, where Y represents the brightness, I and Q denote color informations. Get the mean values of the three channels, $\overline{Y}$, $\overline{I}$, $\overline{Q}$. Combine the two color channels according to $\overline{C} = \overline{I} + \overline{Q}$. Threshold the regions based on the following rule:

$$mask_c = \begin{cases} 1 & if|Y_c - \overline{Y}| > T_1 or|I_c + Q_C - \overline{C}| > T_2 \\ 0 & if|Y_c - \overline{Y}| < T_3 or|I_c + Q_C - \overline{C}| < T_4 \\ wait & else \end{cases} \tag{4}$$

where, T_1, T_2, T_3, and T_4 are threshold values. In the current system they are set to be 37,16,10,7 respectively. The first two ensure no false CD regions are detected. The last two can decrease the operation areas for later processing. Herein, the RGB is not adopted for its three channels are highly related.

2. *Circular Analysis.* Here, the aim is to label the "$wait$" areas left by the former step. In [5], a small circular area is used to detect distinctive keypoints. Inspired by that, an enlarged circle with radius R and center x_0 is used. Sampling N uniform distributed points along the circle, x_i, $i = 1, ..., N$. Assume C is a counter, it's initial value is 0. For each x_i, if either $|Y_{x_i} - Y_{x_0}| > T_5$ or $|I_{x_i} - I_{x_0}| + |Q_{x_i} - Q_{x_0}| > T_6$ is satisfied, then $C = C + 1$. If the value of C excesses an integer (the default value is 6), then that point is assigned by 1. Here, the default value for T_5 and T_6 are 20 and 7 respectively.

Figure 4. Rectangular features. From left to right are center surrounded, vertical, horizontal, diagonal, anti-diagonal feature. The size of each is $w \times h$. The scale is $s = 0.25$ and the size of the central part is $(2s \cdot w + 1) \times (2s \cdot h + 1)$. The feature value is the mean value of the white part subtracted by that of the black part.

After applying CCA to the foreground pixels (the pixel value is 1) and merging the adjacent blocks, the CD areas are detected. It must be point out that the global threshold and circular analysis are useful to inspect the CD, but they also detect many non-CD areas at the same time. So, each candidate block is enlarged by 8 pixels for further validation.

3. *Maximum Rectangular Feature Based Validation.* In[6] rectangular features are utilized for face detection and recognition successfully and efficiently. Here, five rectangular features are introduced based on the analysis of the CD's common shape (see Fig.5.). Denote the point set of the black and white part of the ith rectangle with $E_-(i,s)$ and $E_+(i,s)$ respectively. The number of each set is expressed as $N_-(i,s) = |E_-(i,s)|$ and $N_+(i,s) = |E_+(i,s)|$, $i = 0, ..., 4$, where s is the scale factor. Assume the image block size is $w \times h$ and the size of the five boxes are equal to that block. For a given scale s, a feature can be calculated according to:

$$\begin{cases} \mu_-(i,s) = \frac{1}{N_-(i,s)} \sum_{x_i \in E_-(i,s)} Y(x_i) \\ \mu_+(i,s) = \frac{1}{N_+(i,s)} \sum_{x_i \in E_+(i,s)} Y(x_i) \\ F_Y(s) = \max_{0 \le i \le 4} |\mu_-(i,s) - \mu_+(i,s)| \end{cases} \tag{5}$$

where $Y(x_i)$ is the brightness value. In the same way, $F_I(s)$ and $F_Q(s)$ can be computed by replacing $Y(x_i)$ with $I(x_i)$ and $Q(x_i)$. $F_I(s)$ and $F_Q(s)$ are fused based on (6) because both of them represent color info,

$$F_C(s) = F_I(s) + F_Q(s) \tag{6}$$

The above processes are proceed on 7 scales, $\{s|s(l) = 0.1 + 0.05 \cdot l, l = 0, 1, ..., 6\}$. The final outputs are,

$$\begin{cases} F_Y = \max_{0 \le l \le 6} F_Y(s) \\ F_C = \max_{0 \le l \le 6} F_C(s) \end{cases} \tag{7}$$

Given a block, if either $F_Y > 37$ or $F_C > 7$ is satisfied, that block is declared as CD region. The meanings of the 5 rectangle are clear, among which the first responds to the cluster structure, the remainder responds to vertical, horizontal, diagonal, anti-diagonal linear object respectively.

D. The Detection of Defects in Metal Area

The reverse side of the gland cover contains metal ring, where may arise rubber overflow and rust. Similar to the first two, the detection process include 2 steps:

1. Segment R_{cover}, extract the metal edges using morphological operators, sample the edge points and fit two

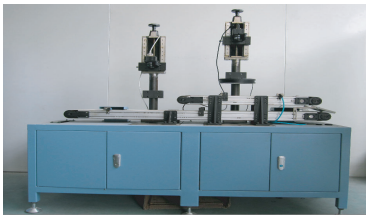

Figure 5. The device of the visual inspection system.

Table I
THE FIELD TEST RESULTS

Defect types	Burr	Color	Rubber	Rust	Total
Ground truth (NO.)	308	58	43	24	433
Detected by Operator(NO.)	300	8	18	3	329
Detected by Machine (NO.)	304	56	43	24	427
Correct Rate Operator (%)	97.40	13.79	41.86	12.50	100
Correct Rate Machine (%)	98.70	96.55	100	75.98	98.61

ellipse models which represent the standard metal contours. Through this step, the rubber overflow and rust processing regions are gained.

2. Extract some efficient features for defect detection. In [7], the authors exploit salient features including combination of colors to detect saliency objects. By observing the defect images, the brightness of areas with rubber overflow defect are lower than the metal areas, thus brightness saliency is used to detect the rubber overflow. When mentioned to rust, a common sense is that the rust component contain with Fe_2O_3, that is the R channel is high. For this reason, the R-B feature is adopted to the rust detection.

III. System and Results

The bearing gland cover inspection system is composed of two MV-3000 cameras, two light sources, a conveyer belta, and so on (see Fig.5.).

Fig.1 shows some typical defect detection results. Fig.1 (a) demonstrates that the MOD feature is efficient for burr detection. The threshold value is set to 0.24, which can suppress the slab-sided contours resulted from model approximation. Fig.1(b) shows that the fixed value is stable to detect CD. Thanks to the gradually refined scheme, the calculation is decreased. Rubber overflow is efficiently detected as is shown in Fig.1 (c), but in Fig.1 (d) some low contrast areas can't be detected entirely, which is not a problem because the users just require to judge whether there is defect other than to know the defect type and size in practices.

Table 1 shows the quantity results of the field test. The total number of the covers is 1016. The ground truth data is obtained through carefully inspection by the expert operators. As the table demonstrated, the performance of the proposed system outperforms the artificial method. The diameter of the cover tested is 80 mm. The precision is chosen for middle grade. Specifically, the sizes of burr, CD, rubber overflow and rust are 0.2mm^2, 0.5mm^2, 2mm^2 and 1mm^2 respectively.

The execution environment of the system is on an Intel Core2 Duo 2.0GHz processor, and all the algorithm is implemented on the plate of vc++ 6.0. The image resolution is $2048*1536$, the average processing time is 0.5s for a gland cover including the image capturing, while the artificial detection time is 1.5s for each.

IV. Conclusion

In this paper, a fast and accuracy visual system has been proposed to detect the defects of covers. The contributions are two fold. The first one is that an intact vision-based system has been developed and put into practical use. The second one is that by analysis the characteristics of the defects, some useful features are proposed to complete the defect detection task efficiently. Field test results demonstrate that the system achieves high performance, solving the online defect detection for covers effectively.

Acknowledgment

The authors would like to thank WUXI BOYANG PRECISION MACHINERY CO.,LTD for providing the research materials and test devices. The authors would also like to thank Yang Gao and Chengfei Zhu for their useful assistance and discussions.

References

[1] K. Wiltschi, A. Pinz and T. Lindeberg, *An automatic assessment scheme for steel quality inspection*. Machine Vision and Applications 12, pp.113-128, 2000.

[2] D.M. Tsai, and T.Y. Huang, *Automated surface inspection for statistical textures*. Image and Vision Computing 21(4), pp.307-323, 2003.

[3] Q. Hu, S. Luo, Y. Qiao and G. Qian, *Supervised grayscale thresholding based on transition regions*. Image Vision Comput 26, pp.1677-1684, 2008.

[4] J. Zhou, F. Chen, and J. Gu, *A Novel Algorithm for Detecting Singular Points from Fingerprint Images*. Pattern Analysis and Machine Intelligence, IEEE Transactions on, vol.31, no.7, pp.1239-1250, July 2009.

[5] S. Smith, and J.M. Brady, *SUSAN-A New Approach to Low Level Image Processing*. Int. J. Comput. Vision 23, pp.45-78, 1997.

[6] P. Viola, and M. Jones, *Rapid object detection using a boosted cascade of simple features*. Proc. Int'l Conf. Computer Vision and Pattern Recognition, 2001.

[7] L. Itti, C. Koch and E. Niebur, *A model of saliency-based visual attention for rapid scene analysis*. Pattern Analysis and Machine Intelligence, IEEE Transactions on, vol.20, no.11, pp.1254-1259, Nov 1998.

[8] E.p. Lyvers, O.R. Mitchell and A.P. Reeves, *Subpixel measurements using a moment-based edge operator*. Pattern Analysis and Machine Intelligence, IEEE Transactions on, vol.11, no.12, pp.1293-1309, Dec 1989.